

The fatty acid elongase ELOVL6 regulates bortezomib resistance in multiple myeloma

Brittany C. Lipchick,^{1*} Adam Utley,^{1*} Zhannan Han,¹ Sudha Moparthy,¹ Dong Hyun Yun,¹ Anna Bianchi-Smiraglia,² David W. Wolff,¹ Emily Fink,² Liang Liu,¹ Cristina M. Furdai,³ Jingyun Lee,³ Kelvin P. Lee,⁴ and Mikhail A. Nikiforov¹

¹Department of Cancer Biology, Wake Forest School of Medicine, Winston-Salem, NC; ²Department of Cell Stress Biology, Roswell Park Comprehensive Cancer Center, Buffalo, NY; ³Section on Molecular Medicine, Department of Internal Medicine, Wake Forest University Health Sciences, Winston-Salem, NC; and ⁴Department of Immunology, Roswell Park Comprehensive Cancer Center, Buffalo, NY

Key Points

- Low levels of fatty acid elongase ELOVL6 are associated with resistance to BTZ in patient and cultured MM cells.
- Changes in the ELOVL6-dependent lipidome modulate response and resistance of MM cells to BTZ.

Resistance to the proteasome inhibitor bortezomib (BTZ) represents a major obstacle in the treatment of multiple myeloma (MM). The contribution of lipid metabolism in the resistance of MM cells to BTZ is mostly unknown. Here we report that levels of fatty acid elongase 6 (ELOVL6) were lower in MM cells from BTZ-nonresponsive vs BTZ-responsive patients and in cultured MM cells selected for BTZ resistance compared with parental counterparts. Accordingly, depletion of ELOVL6 in parental MM cells suppressed BTZ-induced endoplasmic reticulum (ER) stress and cytotoxicity, whereas restoration of ELOVL6 levels in BTZ-resistant MM cells sensitized them to BTZ in tissue culture settings and, as xenografts, in a plasmacytoma mouse model. Furthermore, for the first time, we identified changes in the BTZ-induced lipidome between parental and BTZ-resistant MM cell lines underlying a functional difference in their response to BTZ. We demonstrated that restoration of ELOVL6 levels in BTZ-resistant MM cells resensitized them to BTZ largely via upregulation of ELOVL6-dependent ceramide species, which was a prerequisite for BTZ-induced ER stress and cell death in these cells. Our data characterize ELOVL6 as a major clinically relevant regulator of MM cell resistance to BTZ, which can emerge from the impaired ability of these cells to alter ceramide composition in response to BTZ.

Introduction

Multiple myeloma (MM) is a malignancy of bone marrow plasma cells (PCs) that accounts for ~13% to 15% of all hematological malignancies.¹ In the past decades, significant progress has been achieved in treating MM patients with proteasome inhibitors in combination with immunomodulatory drugs.² However, MM remains largely incurable because of emerging resistance to proteasome inhibitors, the mechanisms of which are not well understood.³

Bortezomib (BTZ),⁴ the first-in-class proteasome inhibitor, has been thought to act primarily through the inhibition of protein degradation, leading to the accumulation of misfolded and unfolded proteins, which subsequently induce endoplasmic reticulum (ER) stress.⁵ ER stress triggers a multifaceted program termed the unfolded protein response (UPR) to restore ER homeostasis.⁶ However, unmitigated ER stress results in cell death, which is activated by the same UPR components.⁷

Importantly, the ER is also a primary site for lipid biosynthesis, and certain lipids have been known to cause lipotoxic ER stress, resulting in the activation of UPR and cell death.⁸ Therefore, it is conceivable that BTZ-induced changes in lipid composition may lead to perturbations in ER homeostasis that

Submitted 4 June 2020; accepted 10 February 2021; published online 6 April 2021.
DOI 10.1182/bloodadvances.2020002578.

*B.C.L. and A.U. contributed equally to this work.

For data sharing, please contact the corresponding author at mnikifor@wakehealth.edu.

The full-text version of this article contains a data supplement.

© 2021 by The American Society of Hematology

contribute to overall BTZ cytotoxicity. Conversely, suppression of such perturbations may represent a mechanism of BTZ resistance.

Among the ER-synthesized lipids, ceramides have been frequently implicated in the induction of apoptosis,⁹ although several reports have demonstrated a prosurvival function of ceramides,¹⁰ making their role in cell survival unclear. Ceramides consist of a sphingosine long-chain base and a fatty acyl chain.¹¹ In mammals, ceramide levels and composition are regulated by ceramide synthases (CERS1-6), which catalyze the coupling of sphinganine to fatty acids (FAs) with variable chain lengths.¹² It has been suggested that the prosurvival vs proapoptotic function of ceramides depends on their FA composition.¹³

ELOVL6 catalyzes the elongation of long-chain saturated and monounsaturated FAs from a chain length of 16 to 18 carbon atoms.¹⁴ The involvement of ELOVL6 in regulation of cell death seems to be controversial, with different articles reporting that both depletion/deficiency and overexpression of ELOVL6 may cause lipotoxicity as a result of the perturbed balance of saturated and monosaturated C16 or C18 FAs.¹⁵⁻¹⁸ The role of lipid metabolism in resistance of MM cells to BTZ is virtually unknown,^{19,20} as is the function of ELOVL6 in the regulation of ceramide composition as a mediator of BTZ-induced ER stress and cell death. Here, we combined patient- and cell line-based gene expression profiling with lipidomic and functional genetic analyses and identified ELOVL6 as a clinically relevant regulator of BTZ resistance in MM.

Methods

Cell lines

Parental and resistant human MM cells RPMI8226, ANBL-6, and KAS6/1 were a gift from Robert Z. Orlowski (MD Anderson Cancer Center).²¹ Human MM cell lines MM.1S, RPMI-8226, KMS11, and ARH77 were purchased from American Type Culture Collection. HEK293FT cells were purchased from Clontech (Mountain View, CA) and cultured in Dulbecco's modified Eagle medium (Invitrogen, Carlsbad, CA) supplemented with 10% fetal bovine serum (FBS), 2 mM glutamine, and penicillin-streptomycin antibiotics. MM cells were cultured in RPMI (Invitrogen), supplemented with 10% FBS or 10% delipidated FBS, 2 mM glutamine, 10 mM *N*-2-hydroxyethylpiperazine-*N'*-2-ethanesulfonic acid (pH, 7.4), nonessential amino acids, 1 mM sodium pyruvate, and penicillin-streptomycin antibiotics. To generate BTZ-resistant cell lines (MM.1S-R, RPMI-8226-R, KMS11-R, and ARH77-R), naïve MM cells were cultured in the presence of increasing concentrations of BTZ (from 1 to 8 nM) for over 6 months. During this period, media and BTZ were replenished every 2 to 3 days. Naïve cells were passaged for the same period of time in BTZ-free media. Resistant cells were maintained in BTZ-free media for at least 3 weeks before being used in the experiments. All cell lines were authenticated and verified as mycoplasma free using the MycoAlert mycoplasma detection kit (catalog #LT07-318; Lonza, Allendale, NJ).

Cell viability assays

MM cells were seeded at 2×10^5 cells per mL in 12-well plates and treated with the indicated BTZ doses. At the indicated time points, cell viability was assessed by live cell counts with trypan blue exclusion or either a SYTOX (SYTOX Dead Cell Stains Protocol; Thermo Fisher Scientific, Waltham, MA) or WST-1 assay (Millipore

Sigma). Experiments were performed in triplicates and repeated at least two times.

For SYTOX, cells were harvested into 5-mL flow cytometric tubes and washed in phosphate-buffered saline (PBS), spinning down at 1400 rpm for 4 minutes. Supernatant was decanted, and cells were resuspended in 200 μ L of PBS with a 1:1000 dilution of the SYTOX stain. Cells were incubated for 20 minutes at room temperature in the dark and taken immediately for flow cytometric analysis using a BD FACSCanto II as per manufacturer instructions; 10 000 events were recorded per sample.

For the WST-1 assay, cells were harvested into 1.5-mL centrifuge tubes and spun at 2000 rpm for 5 minutes. Media was aspirated off, and cells were resuspended in warm RPMI 1640 containing 10% serum at a concentration of 1×10^6 cells per mL; 90 μ L of cell suspension was added to individual wells in a 96-well plate in triplicate, and 10 μ L of WST-1 reagent was added to each well individually. Cells were then incubated at 37°C for 4 hours before spectrophotometric evaluation of absorbance as per manufacturer instructions.

Reagents

BTZ was purchased from Selleckchem (Houston, TX) and dissolved in dimethyl sulfoxide. Ceramides were purchased from Avanti Polar Lipids (Alabaster, AL). Ceramides were added to the media as a 50% ethanol solution in water.

Immunoblotting

Whole-cell extracts were prepared and analyzed as previously described.²² The following antibodies were used: ELOVL6 (ABS458; EMD Millipore; 1:300 dilution), sterol regulatory element binding transcription factor 1 (SREBP1; SC-367; Santa Cruz Biotechnology; 1:500), glyceraldehyde-3-phosphate dehydrogenase (HRP-60004; Proteintech; 1:2500), BiP (3177; Cell Signaling; 1:500), ATF4 (10835-1-AP; Proteintech; 1:1000), and XBP1s (SC-8015; Santa Cruz Biotechnology; 1:500).

Plasmids and infection

The pCMVdeltaR8.2 and pCMV-VSV-G vectors were purchased from Addgene (Cambridge, MA). The pLV-SV4-puro lentiviral vector was obtained from Peter Chumakov (Cleveland Clinic, Cleveland, OH). SREBP1 short hairpin RNAs (shRNAs; TRCN0000422088 and TRCN0000434619) and ELOVL6 shRNAs (TRCN0000278466 and TRCN0000278463) were purchased from Millipore Sigma (Burlington, MA). SREBP1 ORF lentiviral vector was purchased from Addgene (32017). ELOVL6 ORF lentiviral vector (EX-T0392-Lv105) was purchased from GeneCopoeia (Rockville, MD). Infections were performed as previously described.²²

Quantitative real-time PCR

Total cellular RNA was isolated using the RNeasy Mini Kit (Qiagen, Valencia, CA). Complementary DNA (cDNA) was prepared using a cDNA reverse transcription kit (Invitrogen). Quantitative reverse transcription polymerase chain reaction (PCR) was performed on the QS6 Fast Real-Time PCR System (Thermo Fisher Scientific) using either SYBR Green Master Mix or TaqMan Master Mix (Invitrogen) and the following probes and primers: Hs-CERS5-Fwd 5'-tattgccaaaccctgtgcac, Hs-CERS5-Rev 5'-aatccagctgctttgacagg, Hs-CERS6-Fwd 5'-acaaattgctccgcccaat, and Hs-CERS6-Rev

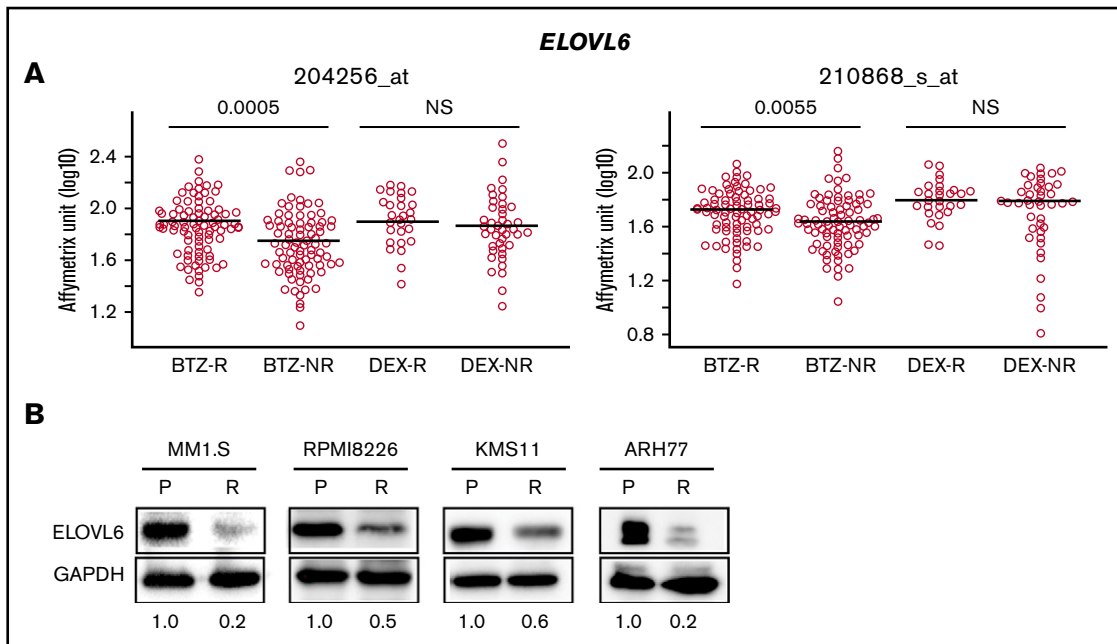


Figure 1. Expression of ELOVL6 correlates with response to BTZ in MM patients and resistance to BTZ in cultured MM cells. (A) Expression of *ELOVL6* in patient MM cells was determined using the GSE9782 data set between patients responsive (R) or nonresponsive (NR) to BTZ (R, n = 85; NR, n = 78) or dexamethasone (DEX) (R, n = 28; NR, n = 39). Probes for *ELOVL6* were extracted based on the annotation from Affymetrix (shown above the plots). The 2-tailed Wilcoxon/Mann-Whitney test was used to determine statistical significance. *P* values between R and NR are shown above each therapy group. (B) Parental and BTZ-resistant MM cell lines with the following BTZ 50% inhibitory concentrations were used: MM.1S-P, 6 nM; MM.1S-R, 10 nM; RPMI8226-P, 3 nM; RPMI8226-R, 15 nM; KMS11-P, 6 nM; KMS11-R, 20 nM; ARH77-P, 8 nM; and ARH77-R, 25 nM. BTZ-resistant cells were collected 3 weeks after selection. Total cell extracts of logarithmically growing parental (P) and BTZ-resistant (R) cells were probed in immunoblotting with designated antibodies. *ELOVL6*-specific signals were normalized by glyceraldehyde-3-phosphate dehydrogenase (GAPDH)-specific signals and by ratio of these signals in corresponding parental cells. Shown immunoblots are representative images of at least 2 independent experiments. NS, nonsignificant.

5'-aaaccagcgcgtgaatgcttc. PCR data were analyzed using QuantStudio Real-Time PCR software (Thermo Fisher Scientific).

Untargeted lipidomic analysis

Measurements were performed in independent biological triplicates. Genetically modified untreated cells were growing exponentially before collection. BTZ-treated cells were collected at least 8 hours before the onset of cell death. Cell death was assessed by trypan blue before collection and never exceeded cell death in control populations. Approximately 10^6 cells were suspended in 200 μ L of methanol and transferred to a tube containing 0.8-mm glass beads; 400 μ L of chloroform was added to the tube, which was mixed using a bead mill homogenizer for lipid extraction. The supernatant isolated by centrifugation at $16\,000\times g$ for 5 minutes was dried under nitrogen at room temperature. The residue was reconstituted in 100 μ L of isopropyl alcohol/methanol (1:1) for lipidomic analysis. Liquid chromatography–tandem mass spectrometry (MS) analysis was performed on a high-resolution Q Exactive HF Hybrid Quadrupole-Orbitrap mass spectrometer (Thermo Fisher Scientific) equipped with the Heated Electrospray Ionization II source (Thermo Fisher Scientific, Rockford, IL) and coupled with the Vanquish UHPLC System (Thermo Fisher Scientific). Ion source parameters were as follows: sheath gas flow rate, 40 L per minute; auxiliary gas flow rate, 5 L per minute; spray voltage, 3.5 and 3.0 kV for the positive and negative modes, respectively; capillary temperature, 350°C; and S-lens radiofrequency voltage, 75 V. The chromatographic separation of lipids was performed on

the Accucore C30 column (3×150 mm; 2.6 μ m) using a linear gradient with 60:40 acetonitrile/water (mobile phase A) and 90:10 isopropyl alcohol/acetonitrile (mobile phase B), both of which contain 0.1% formic acid and 10 mM ammonium formate. MS spectra were acquired by data-dependent scans in positive and negative modes. A survey scan was performed at the MS1 level to identify the top-10 most abundant precursor ions, followed by MS2 scans where product ions were generated from selected ions. High-energy collisional dissociation was used for ion fragmentation, with stepped collision energy of 25/30 and 30/50/100 eV in each positive and negative polarity. The dynamic exclusion option was enabled during data-dependent scans to enhance compound identification in complex mixture. Acquired spectra were processed using LipidSearch software (version 4.2; Thermo Fisher Scientific, Rockford, IL), with selection of the following classes of lipids: lysophosphatidylcholine, phosphatidylcholine, lysophosphatidylethanolamine, phosphatidylethanolamine, lysophosphatidylserine, phosphatidylserine, lysophosphatidylglycerol, phosphatidylglycerol, lysophosphatidylinositol, phosphatidylinositol, lysophosphatidic acid, phosphatidic acid, sphingomyelin, phytosphingosine, monoglyceride, diglyceride, triglyceride, (O-acyl)-1-hydroxy FA, cardiolipin, sphingosine, sphingosine phosphate, glucosylsphingosine, monoglycosylceramide, diglycosylceramide, triglycosylceramide, ceramides, monosialotetrahexosylganglioside, cholesteryl ester, zymosteryl, stigmasteryl ester, sitosteryl ester, coenzymes, monogalactosylmonoacylglycerol, monogalactosyldiacylglycerol, digalactosylmonoacylglycerol, digalactosyldiacylglycerol, sulfoquinovosylmonoacylglycerol, and

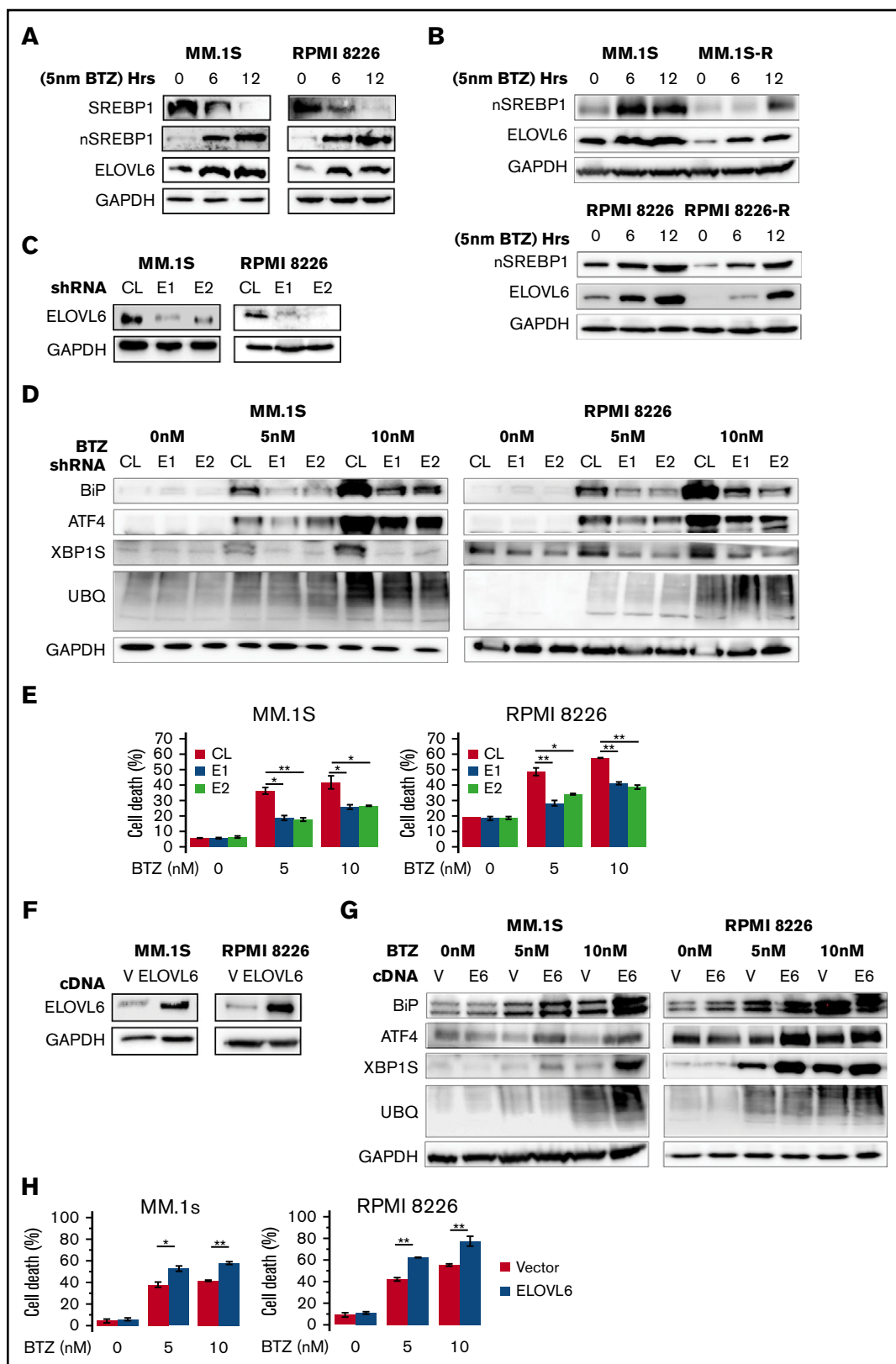


Figure 2. ELOVL6 regulates resistance to BTZ in MM cells. (A-B) MM cells were treated or not with BTZ for the indicated time periods followed by immunoblotting with the indicated antibodies. (C) MM cells were transduced with control (CL) or ELOVL6 shRNAs (E1 or E2) followed by immunoblotting with the indicated antibodies 48 hours postinfection. (D) Cells described in panel C were treated for 16 hours with the indicated amounts of BTZ and probed in immunoblotting with the indicated antibodies (before the onset of cell death). (E) Cells described in panel C were treated with the indicated amounts of BTZ for 24 hours and probed in trypan blue cell viability assay. (F) MM cells

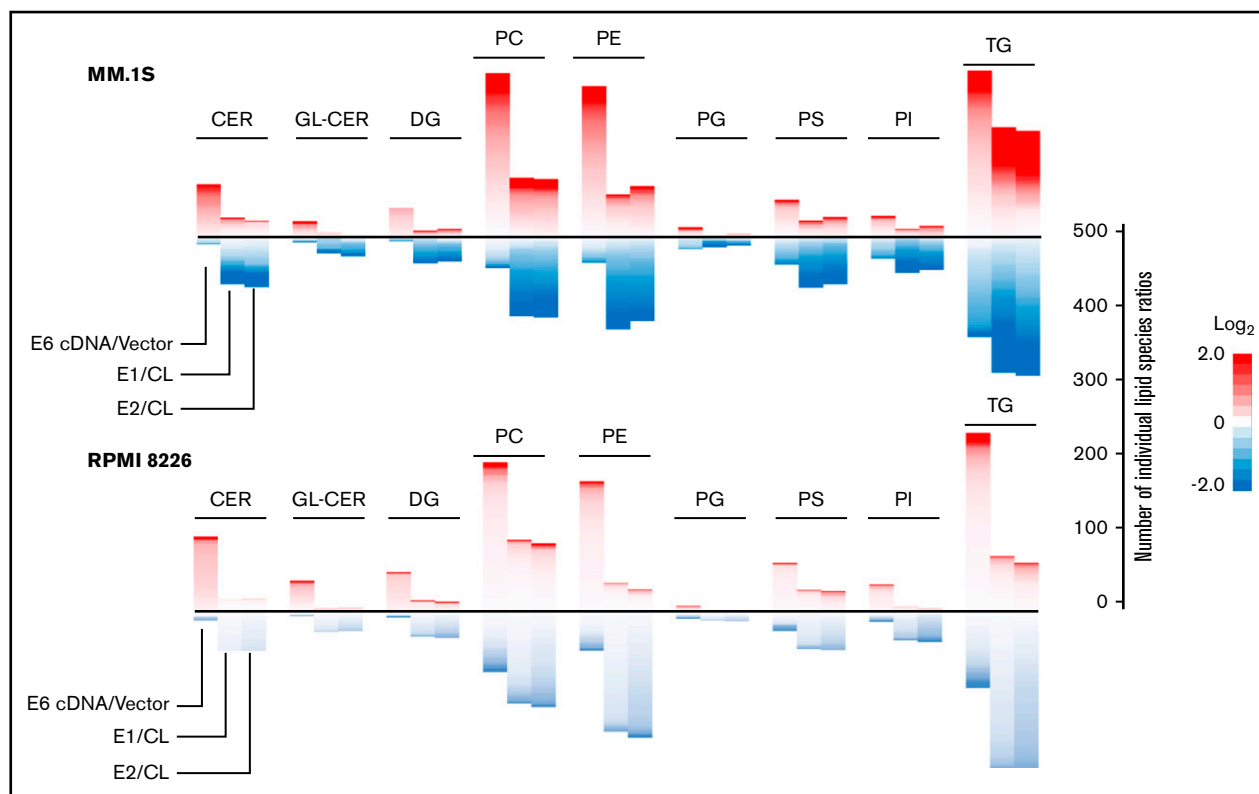


Figure 3. ELOVL6 regulates resistance to BTZ in MM cells. MM.1S and RPMI8226 cells were transduced with empty vector (vector), ELOVL6 cDNA-expressing vector (E6 cDNA), control shRNA (CL), or ELOVL6 shRNAs (E1 or E2). The resulting cell populations were subjected to lipidomic analysis in independent triplicates 48 hours post-infection. Shown are means of the individual lipid ratios between MM cell populations that were calculated and plotted as heatmaps for the following lipid classes using Microsoft R Open (version 3.5.1) software: –ceramides (CER), glycosylceramides (GL-CER), diacylglycerides (DG), –phosphatidylcholine (PC), –phosphatidylethanolamine (PE), –phosphatidylglycerol (PG), –phosphatidylserine (PS), –phosphatidylinositol (PI), and –triglycerides (TG). Only lipid classes with >20 species per lipid class are shown. The heatmaps consist of individual lipid species ratios. A scale for the number of individual lipid species ratios is shown on the right.

sulfoquinovosyldiacylglycerol. Parameters for the product search workflow were as follows: precursor mass tolerance, 5 ppm; product mass tolerance, 5 ppm; product ion intensity threshold, 1.0% relative to precursor; and matching score threshold, 2.0. For FA identification, data were searched with a single selection of only FA class in the database with following parameters: product ion intensity threshold, 0.1% relative to precursor; and matching score threshold, 0.

Experiments with mice

All experiments involving animals were approved by the Institutional Animal Care and Use Committee. Genetically modified MM.1S and RPMI 8226 cells (5.0×10^6 cells per flank) were inoculated subcutaneously in both flanks of 4- to 6-week-old female NOD/Shi-scid interleukin-2 receptor γ null (NOG) mice ($n = 5$ per group). When tumors reached a volume of approximately 100 mm^3 , the animals were randomized to 1 of 2 groups ($n = 5$ per group) and treated with daily intraperitoneal injections of vehicle in PBS or BTZ

in PBS (0.5 mg/kg). Tumor volumes were recorded every 2 days, and mice were euthanized when the tumor volume reached 2 cm^3 or when a tumor became ulcerated.

Statistical analysis and databases

Each experiment was performed at least 2 independent times, and the results are expressed as average \pm standard errors of the mean unless otherwise noted. Statistical analysis was performed using Student *t* test. A 2-tailed *P* value $< .05$ was considered statistically significant for all analyses. Gene expression data along with annotations were downloaded from the National Center for Biotechnology Information Gene Expression Omnibus database (GSE9782) and analyzed as we previously reported.²³ The responder and nonresponder populations within each therapy group were compared using the 2-tailed Wilcoxon/Mann-Whitney test to determine statistical significance. Microsoft R Open (version 3.5.1) software was used for hierarchical clustering and heatmap generation.

Figure 2. (continued) were transduced with empty lentiviral vector (V) or lentiviral vector expressing ELOVL6 cDNA (ELOVL6) followed by immunoblotting with indicated antibodies 48 hours postinfection. (G) Cells described in panel F were treated for 16 hours with the indicated amounts of BTZ and probed in immunoblotting with the indicated antibodies (before the onset of cell death). (H) Cells described in panel F were treated for 24 hours with indicated amounts of BTZ and probed in trypan blue cell viability assay. Shown immunoblots are representative images of at least 2 independent experiments with no tangible experimental variability. The viability data are presented as the mean values of triplicates \pm standard errors of the mean. *P* values were determined by Student *t* test. **P* $< .05$, ***P* $< .01$.

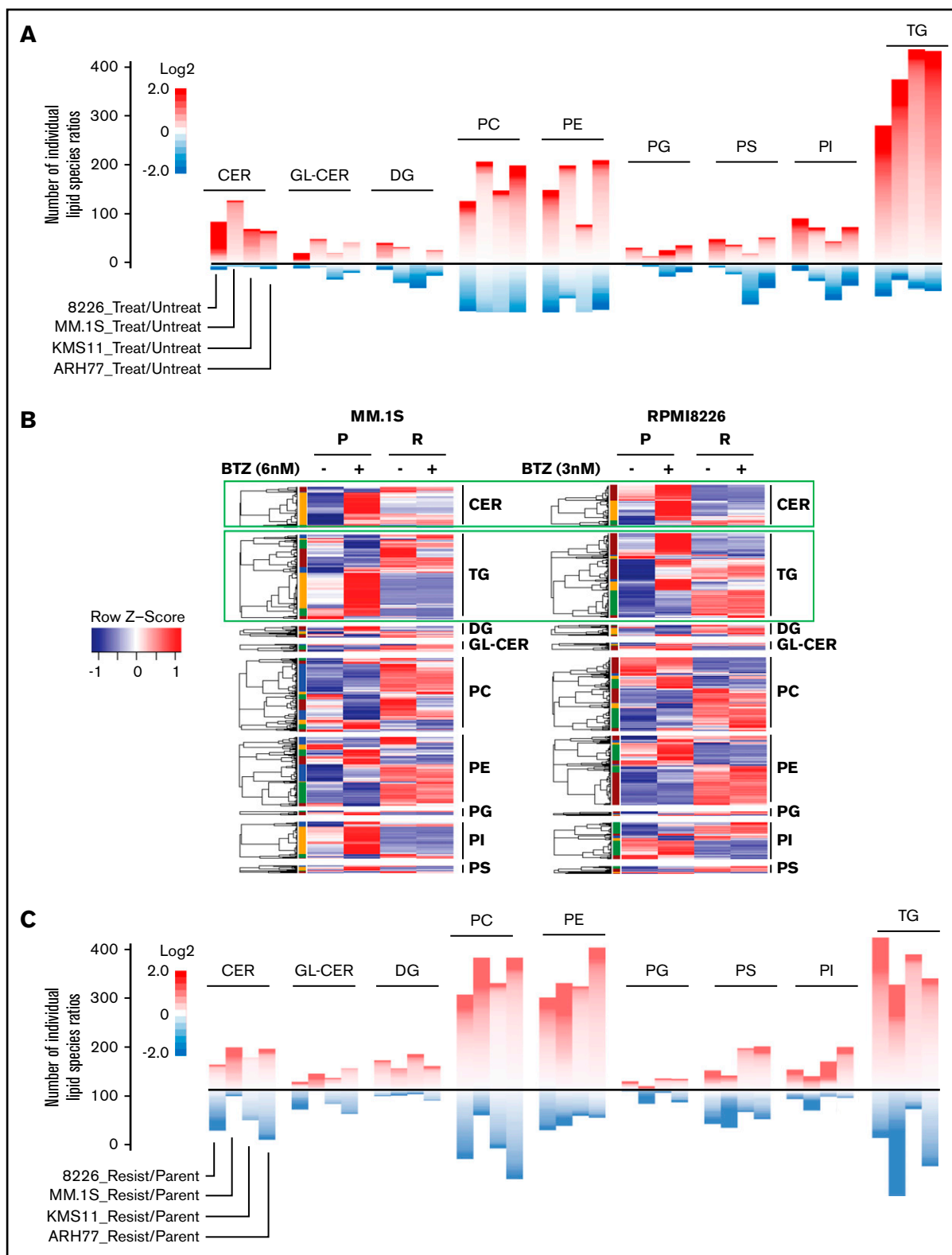


Figure 4. BTZ treatment affects lipid composition in parental and BTZ-resistant MM cells differently. (A) Cells from indicated parental MM cell lines were treated or not with the 50% inhibitory concentration amounts of BTZ for 16 hours (MM.1S, 6 nM; RPMI8226, 3 nM; KMS11, 6 nM; and ARH-77, 8 nM) followed by the assessment of cell viability via trypan blue exclusion assay. No increase in cell death was detected in BTZ-treated cells (data not shown). Treated and untreated cells were subjected to lipidomic analysis in independent triplicates. Mean ratios of the levels of individual lipids between BTZ-treated and untreated MM cells were calculated and plotted as heatmaps for lipid classes designated as in Figure 3. The heatmaps consist of individual lipid species ratios. A scale for the number of individual lipid species ratios is shown on the right.

Results

Decreased levels of ELOVL6 in MM cells correlate with resistance to BTZ in MM patients and cell lines

To identify genes involved in the regulation of BTZ resistance, we used a twofold approach. First, we performed a global RNA sequencing–based gene expression analysis in 3 cell line pairs of previously reported parental and BTZ-resistant MM cell lines (RPMI8226, ANBL-6, and KAS61).²¹ Next, we overlapped the list of genes whose expression significantly changed in at least 2 of 3 cell line pairs (supplemental Table 1) with the list of genes associated with response to BTZ in MM patients²⁴ (supplemental Table 2). The latter list was generated using a data set that contained information on global gene expression in MM cells collected before patient treatment with BTZ or dexamethasone that was correlated with patient response to the drugs.²⁴

As a result, 70 genes were identified whose expression levels were different with high statistical significance in BTZ-resistant vs parental MM cell lines and in MM cells from BTZ-nonresponsive vs BTZ-responsive patients (supplemental Table 3). Of note, among genes downregulated in patient- and cell line–based databases was transcription factor KLF9, which has been shown to mediate BTZ cytotoxicity in MM cells²³ (supplemental Table 3). Furthermore, the transcription factor IRF4, which has been associated with resistance to BTZ,²⁵ was among the genes upregulated in both databases (supplemental Table 3). In addition, 2 of the identified genes control de novo biosynthesis of FAs (ELOVL6²⁶ and FA desaturase 1²⁷). Both genes were downregulated in BTZ-resistant MM cells and in MM cells from BTZ-nonresponsive patients (supplemental Tables 1 and 3). *ELOVL6* expression was also undetectable in a majority of primary samples taken from MM patients in contrast to normal PCs and cells isolated from patients with smoldering myeloma or monoclonal gammopathy of unknown significance (supplemental Figure 1).

We were intrigued by the possibility that alterations in FA metabolism regulate MM resistance to BTZ, because this biological pathway or lipid metabolism in general has not been functionally implicated in MM resistance to proteasome inhibitors. For further analysis, we focused on *ELOVL6* because of its central role in metabolism of the 2 most abundant saturated and monounsaturated FAs (C16 and C18)¹⁴ and the fact that *ELOVL6* levels differed with the highest statistical significance between MM cells from BTZ-responsive and BTX-nonresponsive MM patients according to a Wilcoxon/Mann-Whitney test (Figure 1A; supplemental Table 3). At the same time, no difference in *ELOVL6* levels were detected between MM patients responsive or nonresponsive to dexamethasone treatment (Figure 1A).

Furthermore, transcriptomic analysis demonstrated that *ELOVL6* expression was undetectable in a majority of primary samples taken from MM patients in contrast to normal PCs and cells isolated from

patients with smoldering myeloma or monoclonal gammopathy of unknown significance (supplemental Figure 1), suggesting *ELOVL6* plays a role in MM progression.

To independently validate the gene expression data, we selected 4 MM cell lines (MM.1S, RPMI8226, KMS11, and ARH77) for resistance to the respective 50% inhibitory concentrations of BTZ. After completion of the selection, BTZ-resistant cells were propagated without BTZ for at least 3 weeks without loss of resistance to the drug or increase in the levels of *ELOVL6* (data not shown). *ELOVL6* expression levels were downregulated in all 4 BTZ-resistant cell lines (Figure 1B), suggesting that similar mechanisms of cell-intrinsic resistance to BTZ occur in both patient-derived and cultured MM cells.

ELOVL6 regulates BTZ-induced cell death

ELOVL6 is a bona fide transcriptional target of SREBP1,²⁸⁻³⁰ which is embedded in the ER membrane in its inactive form.³¹ In response to ER stress, SREBP1 undergoes proteolytic cleavage, which generates transcriptionally active nuclear SREBP1 (nSREBP1).³²⁻³⁴ We confirmed that in MM cells, overexpression or depletion of SREBP1 upregulated or downregulated *ELOVL6*, respectively (supplemental Figure 2). Consistently, we demonstrated that levels of *ELOVL6* and nSREBP1 were induced by BTZ treatment of MM.1S and RPMI8226 cells (Figure 2A). Furthermore, resistant MM cells demonstrated lower basal levels of nSREBP1 and the impaired ability to upregulate nSREBP1 and *ELOVL6* in response to BTZ (Figure 2B), suggesting a possible mechanism of *ELOVL6* downregulation in these cells.

We hypothesized that depletion of *ELOVL6* renders MM cells resistant to BTZ. To test this hypothesis, we transduced MM.1S and RPMI8226 cells independently with lentiviral vectors bearing control or 2 different *ELOVL6*-specific shRNAs (Figure 2C). In both cell lines, *ELOVL6* depletion decreased BTZ-induced ER stress (Figure 2D) and cell death (Figure 2E) without suppressing the activity of BTZ (as evidenced by the degree of ubiquitination in BTZ-treated control cells and *ELOVL6*-depleted cells; Figure 2D). Conversely, *ELOVL6* overexpression (Figure 2F) increased BTZ-induced ER stress and cell death in both cell lines as compared with an empty vector control (Figure 2G-H; supplemental Figure 3A), without causing any statistically significant increase in cell death by itself (Figure 2H). Moreover, similar effects with respect to cell death were observed in studied MM cells treated with the BTZ next-generation analog carfilzomib (supplemental Figure 3B-C).

ELOVL6 controls FA composition of multiple lipid classes in MM cells

To understand the mechanisms of *ELOVL6*-dependent regulation of BTZ resistance, MM.1S and RPMI8226 cells, transduced with *ELOVL6* cDNA or *ELOVL6* shRNAs in parallel with the corresponding controls, were subjected to Liquid chromatography–tandem MS–based lipidomic analysis. More than 1100 individual lipid

Figure 4. (continued) Only lipid classes with >20 species are shown. (B) Cells from indicated parental and BTZ-resistant MM cell lines were subjected to untargeted lipidomic analysis in independent triplicates. Raw values of each lipid molecule (each row) were transformed as z scores and plotted as heatmaps, with red representing the highest value and blue representing the lowest value. (C) Cells from indicated parental and BTZ-resistant MM cell lines were subjected to lipidomic analysis in independent triplicates. Mean ratios of the levels of individual lipids between BTZ-resistant and parental MM cells were calculated and plotted as heatmaps for lipid classes designated as in Figure 3. Only lipid classes with >20 species per lipid class are shown. The heatmaps consist of individual lipid species ratios. A scale for the number of individual lipid species ratios is shown on the right.

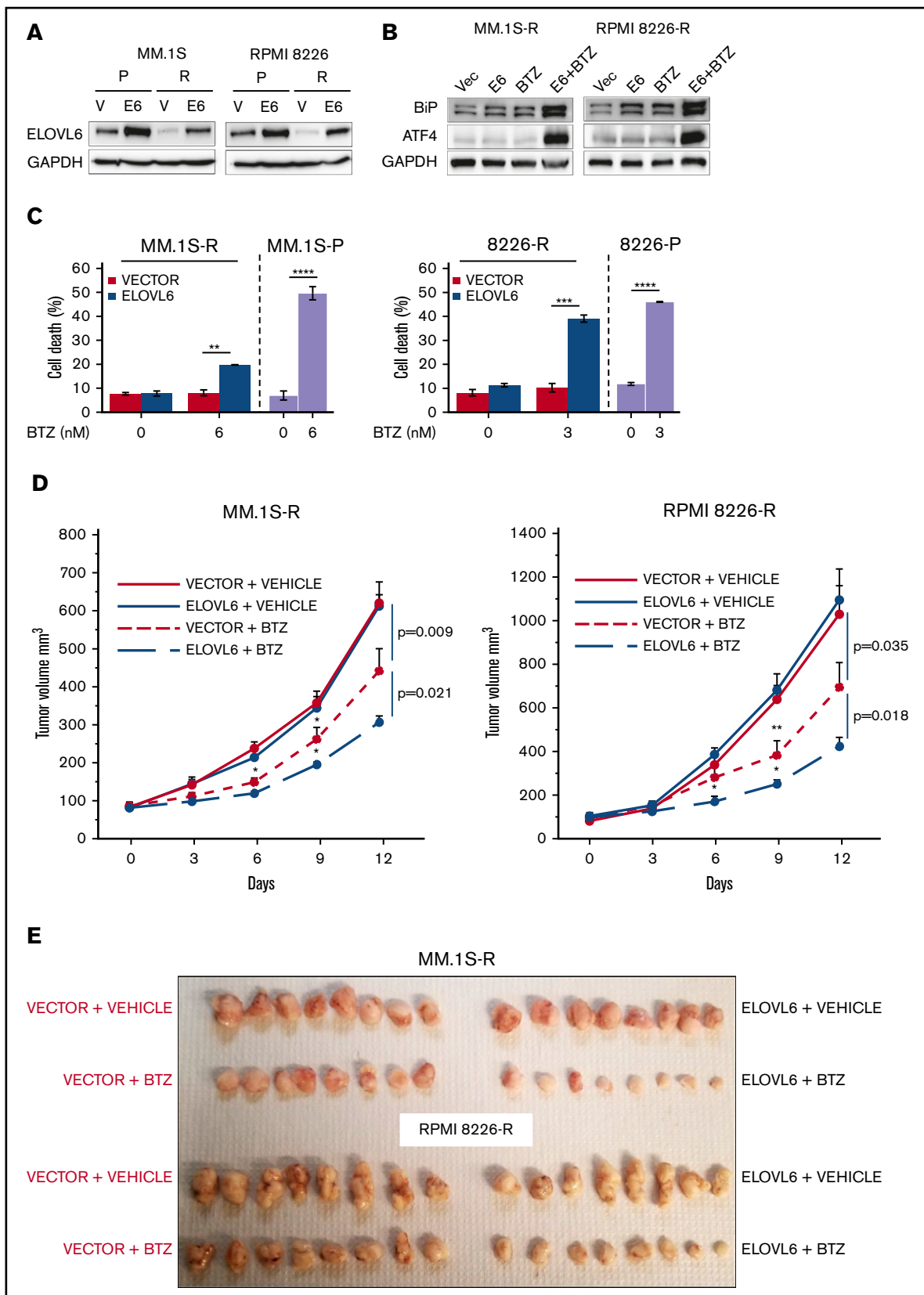


Figure 5. Restoration of ELOVL6 levels in BTZ-resistant cells sensitizes them to bortezomib. (A) Parental (P) and BTZ-resistant (R) MM cells were transduced with empty vector (V) or ELOVL6 cDNA-expressing vector (E6) followed by immunoblotting with indicated antibodies 48 hours postinfection. (B) BTZ-resistant MM.1S and RPMI8226 cells described in panel A were treated or not with 6 nM BTZ or 3 nM BTZ, respectively, for 16 hours followed by immunoblotting with the indicated antibodies.

species were analyzed from multiple lipid classes, including phospholipids, sphingolipids, and glycerolipids (supplemental Table 4). Comparison of lipid profiles in studied cells demonstrated that FA composition across multiple lipid classes depended on ELOVL6 (Figure 3). In addition, the proportion of lipids with fatty acyl chain length ≤ 16 was decreased in ELOVL6-overexpressing cells compared with ELOVL6-depleted cells (supplemental Figure 4), in agreement with the function of ELOVL6 in elongation of C12 to C16 FAs.³⁵

BTZ treatment substantially changes composition of ceramides and triglycerides in parental but not BTZ-resistant cells

Changes in the global lipidome of MM cells in response to proteasome inhibitors have not been studied. To identify such changes, we treated parental and BTZ-resistant MM cell lines with various amounts of BTZ that corresponded to the BTZ 50% inhibitory concentrations of individual parental cell lines and performed untargeted lipidomics before cell death (16 hours posttreatment). The analysis demonstrated that BTZ affected levels of multiple lipid species across all lipid classes in parental cells (Figure 4A). Among those, levels of a majority of ceramide and triglyceride species were substantially upregulated by BTZ in all 4 parental cell lines (Figure 4A). In contrast, no substantial increase in ceramide or triglyceride species was observed in BTZ-resistant cells in response to BTZ treatment (Figure 4B). Interestingly, ceramides and triglycerides were not different among the 4 pairs of BTZ-resistant and parental MM cell lines under untreated (uninduced) conditions (Figure 4C). These findings suggest that the difference in the steady state (ie, uninduced) lipidomes of parental and BTZ-resistant cells may not underlie the resistance to BTZ, which instead may emerge from the impaired ability of BTZ-resistant MM cells to alter lipid composition in response to BTZ.

Restoration of ELOVL6 in BTZ-resistant MM cells resensitized them to BTZ in vitro and in vivo

To test whether ELOVL6 is functionally involved in resistance to BTZ in MM cells, we restored ELOVL6 levels in BTZ-resistant MM.1S and RPMI8226 cells approximately to the levels observed in the corresponding parental cells (Figure 5A). The obtained cell populations, in parallel with cells transduced with an empty vector, were treated or not with BTZ and analyzed for the expression of ER stress markers and the rates of cell death. Neither BTZ treatment nor ELOVL6 overexpression alone caused ER stress or cell death (Figure 5B-C), which were induced only by ELOVL6 overexpression in combination with BTZ treatment (Figure 5B-C). In agreement with these data, ELOVL6 overexpression sensitized tumor xenografts of BTZ-resistant MM.1S and RPMI 8826 cells to BTZ treatment in the plasmacytoma model in NOG mice (Figure 5D-E).

To gain mechanistic insights into the role of ELOVL6 in cell death, we analyzed the composition of BTZ-induced ceramides and triglycerides in BTZ-resistant vector cells and ELOVL6 cells. We demonstrated that BTZ slightly increased levels of a majority of ceramide species in vector cells (Figure 6A-B). ELOVL6 overexpression also caused intermediate upregulation of a majority of ceramide species (Figure 6A-B), whereas ELOVL6 overexpression in combination with BTZ treatment substantially increased ceramide levels (Figure 6A-B). Additionally, BTZ induced expression of ceramide synthases CERS5 and CERS6 in both studied cell lines (supplemental Figure 5), which could synergize with ELOVL6 in total ceramide production.

However, ELOVL6 overexpression did not consistently affect triglyceride levels in studied BTZ-resistant cells; a majority of triglycerides were upregulated in MM.1S cells but not in RPMI8226 cells (supplemental Figure 6A-B). Taken together, these data suggest that ELOVL6 abrogates BTZ resistance in MM cells via upregulation of ceramide species.

ELOVL6-dependent ceramides restore sensitivity of BTZ-resistant MM cells to BTZ

Several recent publications have demonstrated that ceramides may induce or suppress apoptosis caused by various stimuli.^{13,36} Therefore, we were interested in testing whether ceramides upregulated by ELOVL6 mediate BTZ-induced cell death in MM cells. To this end, we arbitrarily chose 2 ceramides (C16 and C18) from the top 10% of ceramide species upregulated by restoration of ELOVL6 in BTZ-resistant MM.1S and RPMI8226 cells (data not shown). Incubation of BTZ-resistant cells with either ceramide (20 μ M for 24 hours [the established conditions used to increase intracellular ceramide levels])^{37,38} did not cause cell death in BTZ-resistant cells (Figure 6C-D). However, treatment of BTZ-resistant cells with C16 or C18 in combination with BTZ significantly increased the levels of ER stress markers and resensitized these cells to BTZ (Figure 6C-D; supplemental Figure 7B-C). In contrast, 24-hour treatment of BTZ-resistant MM cells with 20 μ g/mL of very low density lipoprotein (an established dose for increasing intracellular triglycerides^{39,40}) alone or in combination with BTZ did not induce cell death (Figure 6E).

Taken together, our data identified ELOVL6 as a major regulator of ceramide composition and clinically relevant modulator of BTZ resistance in MM cells.

Discussion

The ER is the primary site for the location of multiple enzymes involved in lipid metabolism and a central organelle for lipid biosynthesis.⁴¹ Because of this, the ER controls the lipid composition and physical properties of all biological membranes, including its

Figure 5. (continued) (C) MM cells described in panel A were treated or not with the indicated amounts of BTZ for 24 hours and probed in trypan blue cell viability assay. Shown immunoblots are representative images of at least 2 independent experiments with no tangible experimental variability. Viability data of parental MM.1S and RPMI8226 cells treated under the same conditions as BTZ-resistant cells are shown for comparison. The viability data are presented as the mean values of triplicates \pm standard errors of the mean. (D) BTZ-resistant MM.1S or RPMI8226 cells transduced with empty vector or ELOVL6 cDNA-expressing vector (as in panel A) and inoculated subcutaneously into both flanks of 4- to 6-week-old female NOG mice. Mice with similar tumor burden were randomized into 2 groups ($n = 5$ animals per group) and treated on days 0, 3, 6, and 9 via intraperitoneal injections with vehicle (PBS) or BTZ in vehicle (0.5 mg/kg). Tumor volumes were recorded on the indicated dates. (E) At the end of the experiments, mice were euthanized, and tumors were excised, fixed in formaldehyde solution, and photographed. Data are presented as the mean values \pm standard errors of the mean. P values were determined by Student t test. * $P < .05$, ** $P < .01$, *** $P < .001$, **** $P < .0001$.

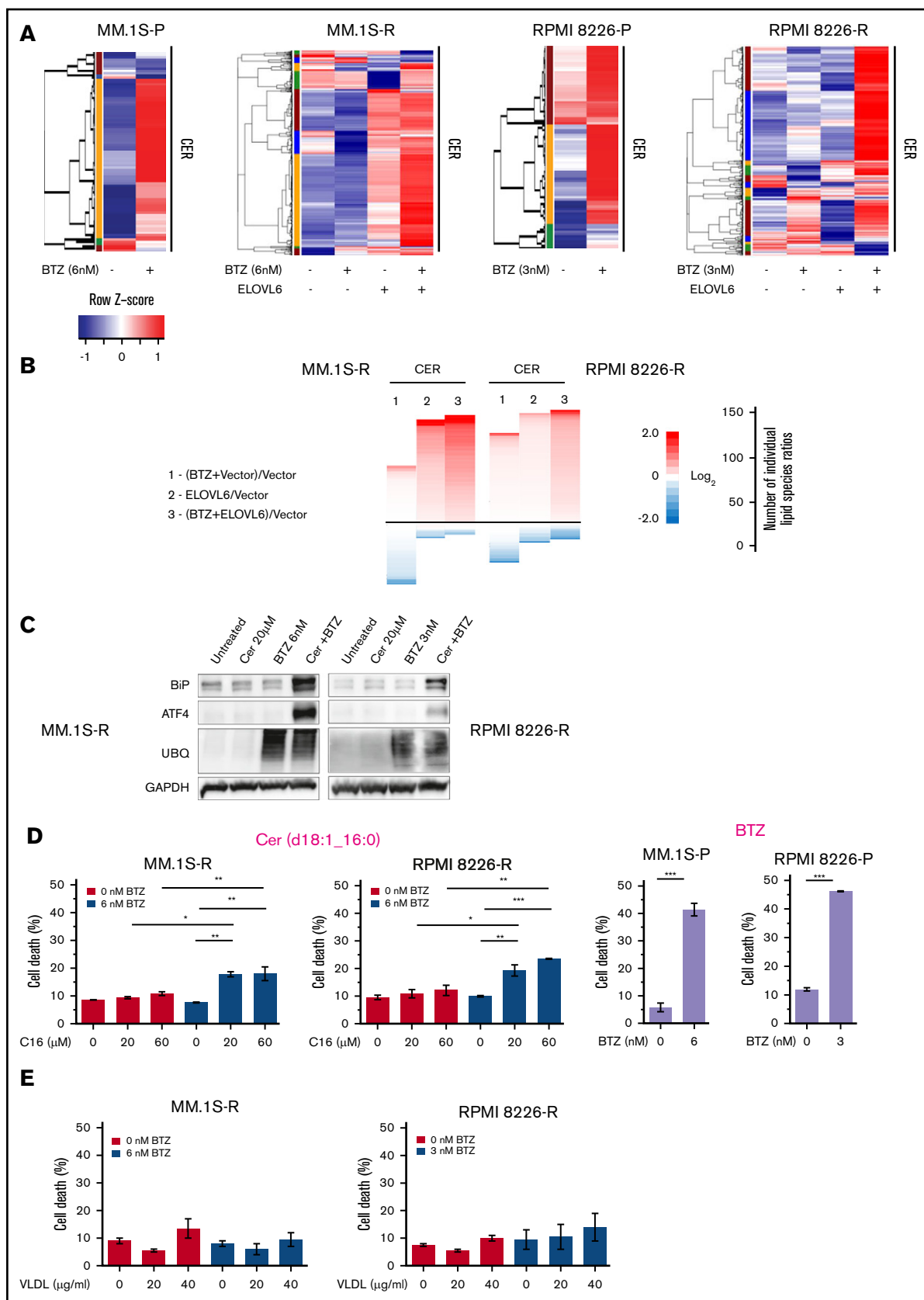


Figure 6. Addition of ceramides (CER) mimics ELOVL6-dependent effects in BTZ-resistant MM cells. (A) Parental (P) and BTZ-resistant (R) MM cells expressing or not empty vector or ELOVL6 were treated or not with the indicated amounts of BTZ for 16 hours followed by lipidomic analysis in independent triplicates. Raw values of each

own.⁴² The cross-talk between lipid metabolism and ER stress has been described in several studies.⁴³ For example, an adaptive response to proteotoxic ER stress activates the transcription factors XBP1S and ATF6,⁴⁴ which in turn upregulate transcription of multiple lipid biosynthesis genes.^{45,46} This provides lipids for the ER membrane expansion, leading to alleviation of ER stress.⁴⁷ Conversely, changes in the lipid composition of the ER membrane may affect protein folding in the ER, thus causing proteotoxic ER stress.^{48,49}

The role of perturbations in lipid metabolism as mediators of BTZ cytotoxicity has not been well investigated. We propose a model whereby BTZ treatment increases ELOVL6 levels via activation of nSREBP1, leading to enhanced production of a vast majority of ceramide species and exacerbation of BTZ-induced ER stress. *SREBP1* is downregulated during the ontological progression of B cells to bone marrow PCs (probe 202308_at; Amazonia database), suggesting that PC survival (and by extension, MM cell survival) is dependent on lower levels of *SREBP1* expression. *SREBP1*-mediated ELOVL6 activation seems to be quantitatively driven to induce MM cell death upon BTZ treatment. Consequently, resistance of MM cells to BTZ is mediated by the diminished ability of MM cells to increase ELOVL6-dependent ceramide production in response to BTZ. This model is supported by several findings, including partial suppression of BTZ-induced ER stress and cell death by depletion of ELOVL6 and the ability of ELOVL6-dependent ceramides to cooperate with BTZ in BTZ-resistant myeloma cells. Of note, although we demonstrated that ELOVL6 regulated the composition of multiple lipid species, including ceramides and triglycerides, BTZ (which also upregulated ELOVL6 levels) most consistently increased levels of ceramides and triglycerides, but not other ELOVL6-dependent lipid species. This could be due to the pleiotropic nature of BTZ activity, which may affect the cell lipidome via modulation of the levels or activity of other lipid metabolism enzymes in addition to ELOVL6.

ELOVL6 mainly elongates C16 to C18 FAs, and endogenous ceramides in MM cells are overwhelmingly composed of FA chains longer than C16 (supplemental Table 4). This observation can explain the increase in a majority of ceramide species by ELOVL6 in MM cells. It is worth noting, however, that BTZ treatment also affected fatty acyl composition of other lipid species, and their contribution to BTZ cytotoxicity or resistance should be the subject of future studies.

Ceramide levels and composition are controlled by ceramide synthases (CERS1-6).^{13,50} In MM cells, BTZ induced expression of only CERS5 and CERS6. The role of these proteins in cancer progression and induction of cell death is controversial. Several publications have suggested that CERS5 may increase proliferation of cancer cells and facilitate progression in colorectal and breast

cancers^{13,51,52} but also facilitate cell death in cancer cells in response to various cytotoxic agents.^{13,53,54} Moreover, elevated levels of CERS5 have been linked to ER stress and autophagy in adenocarcinoma cells.⁵⁵ Similarly, elevated levels of CERS6 have been associated with tumor invasion, metastasis, and poor survival in patients with non-small-cell lung cancer.⁵⁶ On the other hand, CERS6 has been reported to increase sensitivity of cells from multiple cancer cell lines to chemotherapeutic agents.^{13,57,58} Depending on cell type, CERS6 has also been shown either to suppress ER stress or to facilitate it via promotion of ceramide-dependent Ca^{2+} release into the cytosol.^{13,59,60}

Changes in the levels of FAs, which are the substrates for CERS, have not been considered a limiting factor for ceramide biosynthesis. Interestingly, ELOVL1 has been reported to specifically interact with CERS2,⁶¹ whereas ELOVL6 has been shown to bind CERS4.⁶² It has also been suggested that ELOVL6 may modulate CERS4 activity.⁶² It is unclear whether in addition to supplying FAs for incorporation into ceramides, ELOVL6 also modulates activity of ceramide synthases in MM cells.

Ceramides have been implicated in the induction of apoptosis.^{9,12} In addition, abnormal accumulation of ceramides can induce ER stress.⁶³ Conversely, several studies have also demonstrated antiapoptotic functions for ceramides.^{10,54,64} Our data suggest that in MM cells, at least some ELOVL6-dependent ceramides bear pro-ER stress and proapoptotic functions.

The role of lipid metabolism in MM progression and drug resistance is understudied.^{19,20} Therefore, the function of *SREBP1* in MM initiation, progression, and drug resistance remains unknown. In contrast, aberrant lipid metabolism has been well documented to cause disruption of ER homeostasis.⁸ Several reports have revealed that ER stress and activation of unfolded protein response can be directly caused by toxic lipids independently of the accumulation of misfolded proteins.⁴⁹ Proteotoxic and lipotoxic types of ER stress seem interconnected, likely because of the dual role of the ER in protein folding and maturation⁴⁴ and lipid biosynthesis and trafficking.⁴⁹ Furthermore, upregulation of lipid biosynthesis in response to proteotoxic ER stress⁶⁵ strongly suggests the existence of lipid-based mechanisms capable of alleviation of proteotoxic ER stress, although the exact nature of these mechanisms is virtually unknown (other than general ER membrane expansion⁴¹). More studies will be required for the elucidation of such mechanisms for the therapeutic exploitation of these processes in MM resistant to ER stress-inducing drugs.

Additionally, little is known about changes in the lipid composition of patient MM cells and MM cell lines.⁶⁶⁻⁶⁸ Comprehensive untargeted and targeted lipidomic analyses in MM patients was performed in only 1 pilot study conducted among a rather limited set of MM patients.⁶⁸ This study identified that some ceramide species were

Figure 6. (continued) CER species (each row) were transformed as z scores and plotted in the heatmap, with red representing the highest value and blue representing the lowest value. (B) Mean ratios of the levels of individual CER species between designated BTZ-R MM cells were calculated and plotted as heatmaps. Each row represents an individual CER ratio. (C) BTZ-resistant MM.1S-R and RPMI8226-R cells were incubated with d18:1_16:0 CER (20 μM) and/or indicated amounts of BTZ for 16 hours, followed by immunoblotting with indicated antibodies. Shown immunoblots are representative images of at least 2 independent experiments with no tangible experimental variability. (D) BTZ-R MM.1S-R and RPMI8226-R cells were treated or not with the indicated amounts of d18:1_16:0 CER and/or BTZ for 24 hours and probed in trypan blue cell viability assay. (E) BTZ-R MM.1S-R and RPMI8226-R cells were treated for 24 hours with indicated amounts of VLDL and/or BTZ and probed in trypan blue cell viability assay. All viability data are presented as the mean values of triplicates \pm standard errors of the mean. *P* values were determined by Student *t* test. **P* < .05, ***P* < .01, ****P* < .001. VLDL, very low density lipoprotein.

increased in high-risk MM patient samples, whereas several others were downregulated in relapsed/refractory MM specimens. Another study identified higher levels of sphingomyelins in 1 BTZ-resistant and 1 carfilzomib-resistant cell line.⁶⁹ In parallel, genomic analysis of MM patient samples suggested the involvement of sphingolipid metabolism enzymes in regulation of MM cell viability.⁷⁰ In particular, sphingosine kinase 2, which phosphorylates proapoptotic sphingosine into antiapoptotic sphingosine 1 phosphate⁷¹ has been identified as an enzyme required for MM cell survival.^{70,72} Genetic or pharmacological inhibition of sphingosine kinase 2 via the specific small-molecule inhibitor ABC294640⁷³ led to the increased proteasomal degradation of MYC and MCL1 proteins in MM cells and activation of the proapoptotic gene NOXA.⁷⁰ In addition, upregulation of ceramide pools was demonstrated to be an underlying mechanism.⁷²

In summary, our data identify ELOVL6 as a major clinically relevant regulator of ceramide levels and BTZ resistance in MM cells.

Acknowledgments

This work was supported by National Institutes of Health, National Cancer Institute grants CA193981, CA224434, and CA190533; an International Myeloma Foundation Brian D. Novis Senior Research

Grant Award (M.A.N.); and the Wake Forest Baptist Comprehensive Cancer Center Proteomics and Metabolomics Shared Resource, supported by National Cancer Institute Cancer Center Support grant P30CA012197.

Authorship

Contribution: B.C.L., A.U., and M.A.N. designed the experiments; B.C.L., A.U., and M.A.N. wrote the manuscript; B.C.L. and A.U. performed most of the experiments and analyzed the data; S.M., D.H.Y., Z.H., A.B.-S., D.W.W., and E.F. performed some of the experiments; J.L. performed lipidomic analysis; L.L. performed the bioinformatic analysis; C.M.F. and K.P.L. supervised part of the study; M.A.N. conceived the initial hypothesis and supervised the study; and all authors discussed the results and commented on the manuscript.

Conflict-of-interest disclosure: The authors declare no competing financial interests.

ORCID profiles: B.C.L., 0000-0002-7326-0079; D.W.W., 0000-0003-4201-3857; M.A.N., 0000-0001-7868-0518.

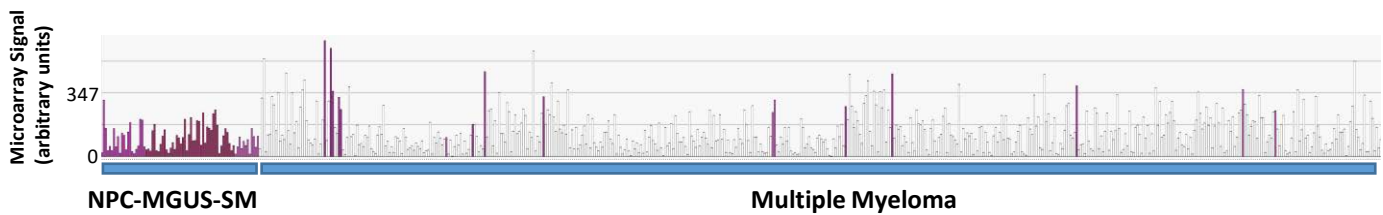
Correspondence: Mikhail A. Nikiforov, Wake Forest School of Medicine, 1 Medical Center Blvd, Winston-Salem, NC 27157; e-mail: mnikifor@wakehealth.edu.

References

1. Multiple myeloma: 2018 update on diagnosis, risk-stratification, and management. *Am J Hematol*. 2018;93(8):981-1114.
2. Gandolfi S, Laubach JP, Hideshima T, Chauhan D, Anderson KC, Richardson PG. The proteasome and proteasome inhibitors in multiple myeloma. *Cancer Metastasis Rev*. 2017;36(4):561-584.
3. Robak P, Drozd I, Szemraj J, Robak T. Drug resistance in multiple myeloma. *Cancer Treat Rev*. 2018;70:199-208.
4. Anderson KC. Bortezomib therapy for myeloma. *Curr Hematol Rep*. 2004;3(1):65.
5. Nikesitch N, Lee JM, Ling S, Roberts TL. Endoplasmic reticulum stress in the development of multiple myeloma and drug resistance. *Clin Transl Immunology*. 2018;7(1):e1007.
6. Schwarz DS, Blower MD. The endoplasmic reticulum: structure, function and response to cellular signaling. *Cell Mol Life Sci*. 2016;73(1):79-94.
7. Obeng EA, Carlson LM, Gutman DM, Harrington WJ Jr., Lee KP, Boise LH. Proteasome inhibitors induce a terminal unfolded protein response in multiple myeloma cells. *Blood*. 2006;107(12):4907-4916.
8. Volmer R, van der Ploeg K, Ron D. Membrane lipid saturation activates endoplasmic reticulum unfolded protein response transducers through their transmembrane domains. *Proc Natl Acad Sci USA*. 2013;110(12):4628-4633.
9. Ogretmen B. Sphingolipid metabolism in cancer signalling and therapy. *Nat Rev Cancer*. 2018;18(1):33-50.
10. Karahatay S, Thomas K, Koybasi S, et al. Clinical relevance of ceramide metabolism in the pathogenesis of human head and neck squamous cell carcinoma (HNSCC): attenuation of C(18)-ceramide in HNSCC tumors correlates with lymphovascular invasion and nodal metastasis. *Cancer Lett*. 2007;256(1):101-111.
11. Hannun YA, Obeid LM. Many ceramides. *J Biol Chem*. 2011;286(32):27855-27862.
12. Mullen TD, Hannun YA, Obeid LM. Ceramide synthases at the centre of sphingolipid metabolism and biology. *Biochem J*. 2012;441(3):789-802.
13. Brachtendorf S, El-Hindi K, Grösch S. Ceramide synthases in cancer therapy and chemoresistance. *Prog Lipid Res*. 2019;74:160-185.
14. Kihara A. Very long-chain fatty acids: elongation, physiology and related disorders. *J Biochem*. 2012;152(5):387-395.
15. Green CD, Olson LK. Modulation of palmitate-induced endoplasmic reticulum stress and apoptosis in pancreatic β -cells by stearoyl-CoA desaturase and Elov6. *Am J Physiol Endocrinol Metab*. 2011;300(4):E640-E649.
16. Sunaga H, Matsui H, Ueno M, et al. Deranged fatty acid composition causes pulmonary fibrosis in Elov6-deficient mice [published correction appears in *Nat Commun*. 2013;4:2937]. *Nat Commun*. 2013;4:2563.
17. Palu RAS, Chow CY. Baldspot/ELOVL6 is a conserved modifier of disease and the ER stress response. *PLoS Genet*. 2018;14(8):e1007557.
18. Shibasaki Y, Horikawa M, Ikegami K, et al. Stearate-to-palmitate ratio modulates endoplasmic reticulum stress and cell apoptosis in non-B non-C hepatoma cells. *Cancer Sci*. 2018;109(4):1110-1120.
19. Masarwi M, DeSchiffart A, Ham J, Reagan MR. Multiple myeloma and fatty acid metabolism. *JBMR Plus*. 2019;3(3):e10173.

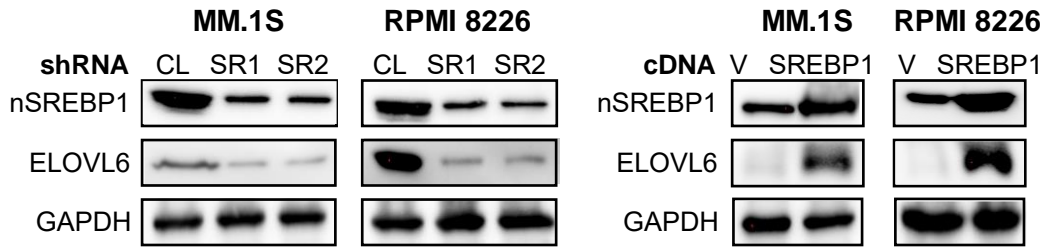
20. Rizzieri D, Paul B, Kang Y. Metabolic alterations and the potential for targeting metabolic pathways in the treatment of multiple myeloma. *J Cancer Metastasis Treat.* 2019;5:26.
21. Kuhn DJ, Berkova Z, Jones RJ, et al. Targeting the insulin-like growth factor-1 receptor to overcome bortezomib resistance in preclinical models of multiple myeloma. *Blood.* 2012;120(16):3260-3270.
22. Fink EE, Mannava S, Bagati A, et al. Mitochondrial thioredoxin reductase regulates major cytotoxicity pathways of proteasome inhibitors in multiple myeloma cells. *Leukemia.* 2016;30(1):104-111.
23. Mannava S, Zhuang D, Nair JR, et al. KLF9 is a novel transcriptional regulator of bortezomib- and LBH589-induced apoptosis in multiple myeloma cells. *Blood.* 2012;119(6):1450-1458.
24. Mulligan G, Mitsiades C, Bryant B, et al. Gene expression profiling and correlation with outcome in clinical trials of the proteasome inhibitor bortezomib. *Blood.* 2007;109(8):3177-3188.
25. Xie Z, Bi C, Chooi JY, Chan ZL, Mustafa N, Chng WJ. MMSET regulates expression of IRF4 in t(4;14) myeloma and its silencing potentiates the effect of bortezomib. *Leukemia.* 2015;29(12):2347-2354.
26. Guillou H, Zdravcov D, Martin PG, Jacobsson A. The key roles of elongases and desaturases in mammalian fatty acid metabolism: Insights from transgenic mice. *Prog Lipid Res.* 2010;49(2):186-199.
27. Lee H, Park WJ. Unsaturated fatty acids, desaturases, and human health. *J Med Food.* 2014;17(2):189-197.
28. Kumadaki S, Matsuzaka T, Kato T, et al. Mouse Elovl-6 promoter is an SREBP target. *Biochem Biophys Res Commun.* 2008;368(2):261-266.
29. Xu HF, Luo J, Zhao WS, et al. Overexpression of SREBP1 (sterol regulatory element binding protein 1) promotes de novo fatty acid synthesis and triacylglycerol accumulation in goat mammary epithelial cells. *J Dairy Sci.* 2016;99(1):783-795.
30. Chen S, He H, Liu X. Tissue expression profiles and transcriptional regulation of elongase of very long chain fatty acid 6 in bovine mammary epithelial cells. *PLoS One.* 2017;12(4):e0175777.
31. Eberlé D, Hegarty B, Bossard P, Ferré P, Foufelle F. SREBP transcription factors: master regulators of lipid homeostasis. *Biochimie.* 2004;86(11):839-848.
32. Zhang C, Chen X, Zhu RM, et al. Endoplasmic reticulum stress is involved in hepatic SREBP-1c activation and lipid accumulation in fructose-fed mice. *Toxicol Lett.* 2012;212(3):229-240.
33. Chen S, Blank JL, Peters T, et al. Genome-wide siRNA screen for modulators of cell death induced by proteasome inhibitor bortezomib. *Cancer Res.* 2010;70(11):4318-4326.
34. Kim H, Moon JY, Burapan S, Han J, Cho SK. Induction of ER stress-mediated apoptosis by the major component 5,7,4'-trimethoxyflavone isolated from kaempferia parviflora tea infusion. *Nutr Cancer.* 2018;70(6):984-996.
35. Moon YA, Shah NA, Mohapatra S, Warrington JA, Horton JD. Identification of a mammalian long chain fatty acyl elongase regulated by sterol regulatory element-binding proteins. *J Biol Chem.* 2001;276(48):45358-45366.
36. Grösch S, Schiffmann S, Geisslinger G. Chain length-specific properties of ceramides. *Prog Lipid Res.* 2012;51(1):50-62.
37. Gao X, Lee K, Reid MA, et al. Serine availability influences mitochondrial dynamics and function through lipid metabolism. *Cell Rep.* 2018;22(13):3507-3520.
38. Rudd AK, Devaraj NK. Traceless synthesis of ceramides in living cells reveals saturation-dependent apoptotic effects. *Proc Natl Acad Sci USA.* 2018;115(29):7485-7490.
39. Tsai YY, Rainey WE, Johnson MH, Bollag WB. VLDL-activated cell signaling pathways that stimulate adrenal cell aldosterone production. *Mol Cell Endocrinol.* 2016;433:138-146.
40. Lupien LE, Bloch K, Dehairs J, et al. Endocytosis of very low-density lipoproteins: an unexpected mechanism for lipid acquisition by breast cancer cells. *J Lipid Res.* 2020;61(2):205-218.
41. Jacquemyn J, Cascalho A, Goodchild RE. The ins and outs of endoplasmic reticulum-controlled lipid biosynthesis. *EMBO Rep.* 2017;18(11):1905-1921.
42. Volmer R, Ron D. Lipid-dependent regulation of the unfolded protein response. *Curr Opin Cell Biol.* 2015;33:67-73.
43. Fun XH, Thibault G. Lipid bilayer stress and proteotoxic stress-induced unfolded protein response deploy divergent transcriptional and non-transcriptional programmes. *Biochim Biophys Acta Mol Cell Biol Lipids.* 2020;1865(1):158449.
44. Hetz C, Papa FR. The unfolded protein response and cell fate control. *Mol Cell.* 2018;69(2):169-181.
45. Wu R, Zhang QH, Lu YJ, Ren K, Yi GH. Involvement of the IRE1 α -XBP1 pathway and XBP1s-dependent transcriptional reprogramming in metabolic diseases. *DNA Cell Biol.* 2015;34(1):6-18.
46. Lebeaupin C, Vallée D, Hazari Y, Hetz C, Chevet E, Bailly-Maitre B. Endoplasmic reticulum stress signalling and the pathogenesis of non-alcoholic fatty liver disease. *J Hepatol.* 2018;69(4):927-947.
47. Schuck S, Prinz WA, Thorn KS, Voss C, Walter P. Membrane expansion alleviates endoplasmic reticulum stress independently of the unfolded protein response [published correction appears in *J Cell Biol.* 2021;220(4):jcb.20090707402092021c]. *J Cell Biol.* 2009;187(4):525-536.
48. Shyu P Jr., Ng BSH, Ho N, et al. Membrane phospholipid alteration causes chronic ER stress through early degradation of homeostatic ER-resident proteins. *Sci Rep.* 2019;9(1):8637.
49. Han J, Kaufman RJ. The role of ER stress in lipid metabolism and lipotoxicity. *J Lipid Res.* 2016;57(8):1329-1338.
50. Levy M, Futerman AH. Mammalian ceramide synthases. *IUBMB Life.* 2010;62(5):347-356.

51. Fitzgerald S, Sheehan KM, Espina V, et al. High CerS5 expression levels associate with reduced patient survival and transition from apoptotic to autophagy signalling pathways in colorectal cancer. *J Pathol Clin Res*. 2014;1(1):54-65.
52. Schifmann S, Sandner J, Birod K, et al. Ceramide synthases and ceramide levels are increased in breast cancer tissue. *Carcinogenesis*. 2009;30(5):745-752.
53. Jin J, Mullen TD, Hou Q, et al. AMPK inhibitor compound C stimulates ceramide production and promotes Bax redistribution and apoptosis in MCF7 breast carcinoma cells. *J Lipid Res*. 2009;50(12):2389-2397.
54. Mesicek J, Lee H, Feldman T, et al. Ceramide synthases 2, 5, and 6 confer distinct roles in radiation-induced apoptosis in HeLa cells. *Cell Signal*. 2010;22(9):1300-1307.
55. Yamane M, Miyazawa K, Moriya S, Abe A, Yamane S. D,L-Threo-1-phenyl-2-decanoylamino-3-morpholino-1-propanol (DL-PDMP) increases endoplasmic reticulum stress, autophagy and apoptosis accompanying ceramide accumulation via ceramide synthase 5 protein expression in A549 cells. *Biochimie*. 2011;93(9):1446-1459.
56. Suzuki M, Cao K, Kato S, et al. Targeting ceramide synthase 6-dependent metastasis-prone phenotype in lung cancer cells. *J Clin Invest*. 2016;126(1):254-265.
57. Walker T, Mitchell C, Park MA, et al. Sorafenib and vorinostat kill colon cancer cells by CD95-dependent and -independent mechanisms. *Mol Pharmacol*. 2009;76(2):342-355.
58. Walker T, Mitchell C, Park MA, et al. 17-allylamino-17-demethoxygeldanamycin and MEK1/2 inhibitors kill GI tumor cells via Ca²⁺-dependent suppression of GRP78/BiP and induction of ceramide and reactive oxygen species. *Mol Cancer Ther*. 2010;9(5):1378-1395.
59. Senkal CE, Ponnusamy S, Manevich Y, et al. Alteration of ceramide synthase 6/C16-ceramide induces activating transcription factor 6-mediated endoplasmic reticulum (ER) stress and apoptosis via perturbation of cellular Ca²⁺ and ER/Golgi membrane network. *J Biol Chem*. 2011;286(49):42446-42458.
60. Yacoub A, Hamed HA, Allegood J, et al. PERK-dependent regulation of ceramide synthase 6 and thioredoxin play a key role in mda-7/IL-24-induced killing of primary human glioblastoma multiforme cells. *Cancer Res*. 2010;70(3):1120-1129.
61. Ohno Y, Suto S, Yamanaka M, et al. ELOVL1 production of C24 acyl-CoAs is linked to C24 sphingolipid synthesis. *Proc Natl Acad Sci USA*. 2010;107(43):18439-18444.
62. Matsuzaka T, Kuba M, Koyasu S, et al. Hepatocyte ELOVL fatty acid elongase 6 determines ceramide acyl-chain length and hepatic insulin sensitivity in mice. *Hepatology*. 2020;71(5):1609-1625.
63. Zelnik ID, Ventura AE, Kim JL, Silva LC, Futerman AH. The role of ceramide in regulating endoplasmic reticulum function. *Biochim Biophys Acta Mol Cell Biol Lipids*. 2020;1865(1):158489.
64. Senkal CE, Ponnusamy S, Bielawski J, Hannun YA, Ogretmen B. Antiapoptotic roles of ceramide-synthase-6-generated C16-ceramide via selective regulation of the ATF6/CHOP arm of ER-stress-response pathways. *FASEB J*. 2010;24(1):296-308.
65. Song MJ, Malhi H. The unfolded protein response and hepatic lipid metabolism in non alcoholic fatty liver disease. *Pharmacol Ther*. 2019;203:107401.
66. Nagata Y, Ishizaki I, Waki M, et al. Palmitic acid, verified by lipid profiling using secondary ion mass spectrometry, demonstrates anti-multiple myeloma activity. *Leuk Res*. 2015;39(6):638-645.
67. Franco D, Trusso S, Fazio E, et al. Raman spectroscopy differentiates between sensitive and resistant multiple myeloma cell lines. *Spectrochim Acta A Mol Biomol Spectrosc*. 2017;187:15-22.
68. Mohamed A, Collins J, Jiang H, et al. Concurrent lipidomics and proteomics on malignant plasma cells from multiple myeloma patients: Probing the lipid metabolome. *PLoS One*. 2020;15(1):e0227455.
69. Besse L, Besse A, Mendez-Lopez M, et al. A metabolic switch in proteasome inhibitor-resistant multiple myeloma ensures higher mitochondrial metabolism, protein folding and sphingomyelin synthesis. *Haematologica*. 2019;104(9):e415-e419.
70. Venkata JK, An N, Stuart R, et al. Inhibition of sphingosine kinase 2 downregulates the expression of c-Myc and Mcl-1 and induces apoptosis in multiple myeloma. *Blood*. 2014;124(12):1915-1925.
71. Zheng X, Li W, Ren L, et al. The sphingosine kinase-1/sphingosine-1-phosphate axis in cancer: Potential target for anticancer therapy. *Pharmacol Ther*. 2019;195:85-99.
72. Wallington-Beddoe CT, Bennett MK, Vandyke K, et al. Sphingosine kinase 2 inhibition synergises with bortezomib to target myeloma by enhancing endoplasmic reticulum stress. *Oncotarget*. 2017;8(27):43602-43616.
73. Sundaramoorthy P, Gasparetto C, Kang Y. The combination of a sphingosine kinase 2 inhibitor (ABC294640) and a Bcl-2 inhibitor (ABT-199) displays synergistic anti-myeloma effects in myeloma cells without a t(11;14) translocation. *Cancer Med*. 2018;7(7):3257-3268.

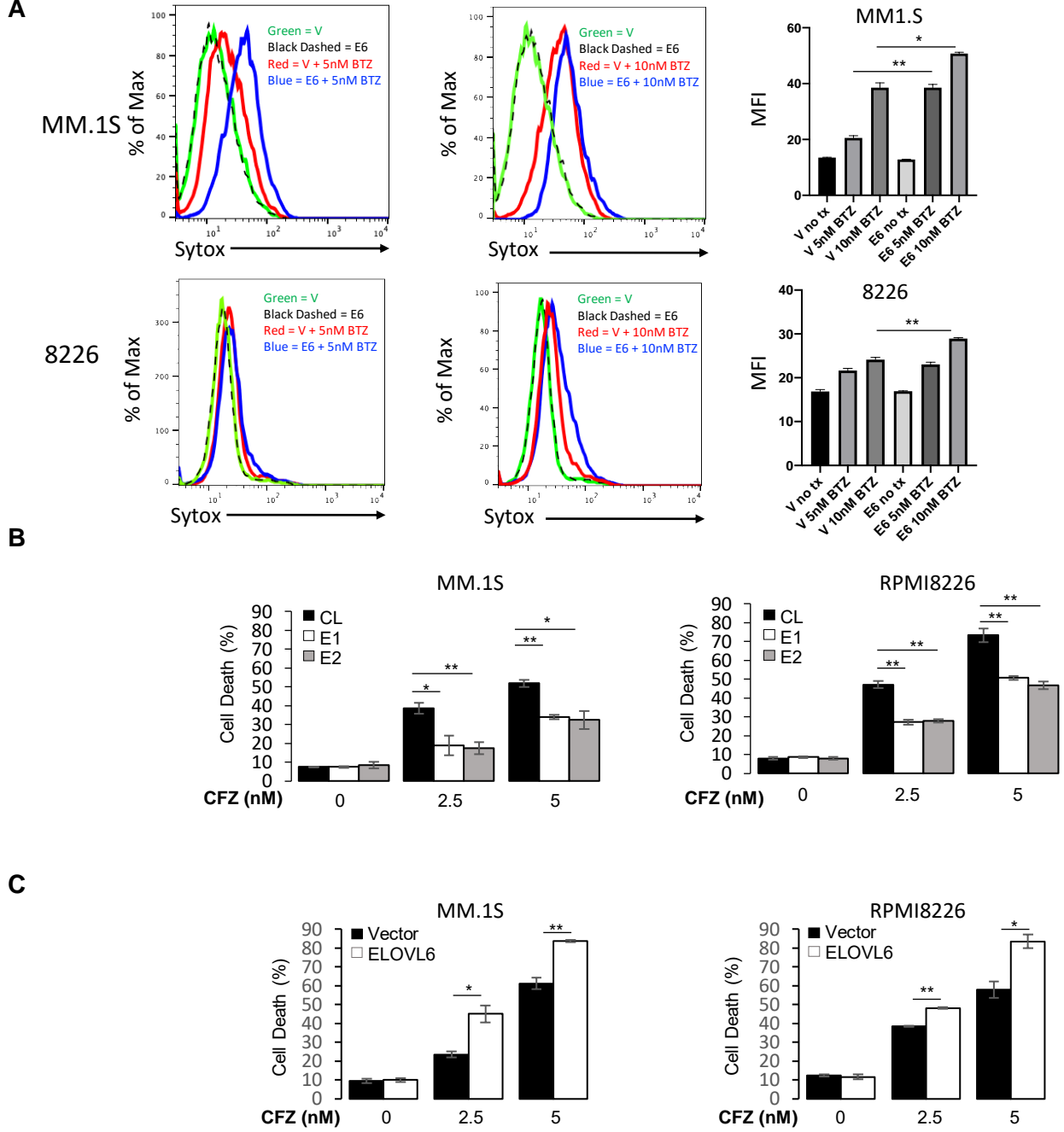


Supplemental Figure 1. *ELOVL6* expression is undetectable in most MM patient samples vs Normal Plasma Cells (NPC), MGUS, and Smoldering Myeloma

Evaluation of *ELOVL6* expression from the Amazonia Gene Expression Atlas in human samples from patients with normal plasma cells (far left), MGUS (second purple shade from left), smoldering myeloma (next purple shade), and multiple myeloma (farthest to the right) using probe 210868_s_at. All colored bars are detected samples, while the white bars indicate “undetectable”. Link to probe dataset description with option to zoom in: http://amazonia.transcriptome.eu/temp/histo_ef5710a1432c560de9aca3bfbe32dc3c.png.



Supplemental Figure 2. SREBP1 regulates *ELOVL6* expression in MM cells. Cells were transduced with the indicated constructs (CL= control ShRNA, SR1=SREBP1 shRNA1, SR2=SREBP1 shRNA2, V=Vector, SERBP1 = SREBP1 cDNA), followed by immunoblotting with the antibodies indicated on the left.



Supplemental Figure 3. ELOVL6 regulates response of MM cells to carfilzomib

A. MM cells were transduced with empty vector (V) or ELOVL6 cDNA (E6) and treated with 5nM, 10nM BTZ for 24hrs. Cell viability was assessed by SYTOX live/dead staining by flow cytometry. Left panels, representative histograms, right, quantification of mean fluorescence intensity of dose-dependent BTZ treated cells. **B.** MM cells were transduced with control (CL) or ELOVL6 shRNAs (E1 or E2). 48hrs post-infection cell populations were treated with the indicated amounts of carfilzomib (CFZ) for 24hrs and probed in trypan blue cell viability assay. **C.** MM cells were transduced with empty vector or ELOVL6 cDNA-expressing vector. 48hrs post-infection cell populations were treated with the indicated amounts of carfilzomib (CFZ) for 24hrs and probed in trypan blue cell viability assay. Data are presented as the mean values \pm S.E.M. * $p < 0.05$, ** $p < 0.01$, by Student's t test.

ELOVL6 depletion increases, whereas ELOVL6 overexpression decreases proportion of C12-C16-containing lipids*

8226

	Among upregulated lipid species	Among downregulated lipid species
ELOVL6 shRNA1/CiShRNA	37.0%	30.6%
ELOVL6 shRNA2/CiShRNA	37.6%	27.6%
ELOVL6 cDNA/Vector	17.8%	28.0%

MM.1S

	Among upregulated lipid species	Among downregulated lipid species
ELOVL6 shRNA1/CiShRNA	32.0%	15.8%
ELOVL6 shRNA2/CiShRNA	31.4%	17.5%
ELOVL6 cDNA/Vector	22.4%	34.0%

* Percent of C18-C26 species equals a difference of 100% and the corresponding percent value of C12-C16 species.

Supplemental Figure 4. Modulation of ELOVL6 levels affects fatty acid distribution in MM cell lipidomes

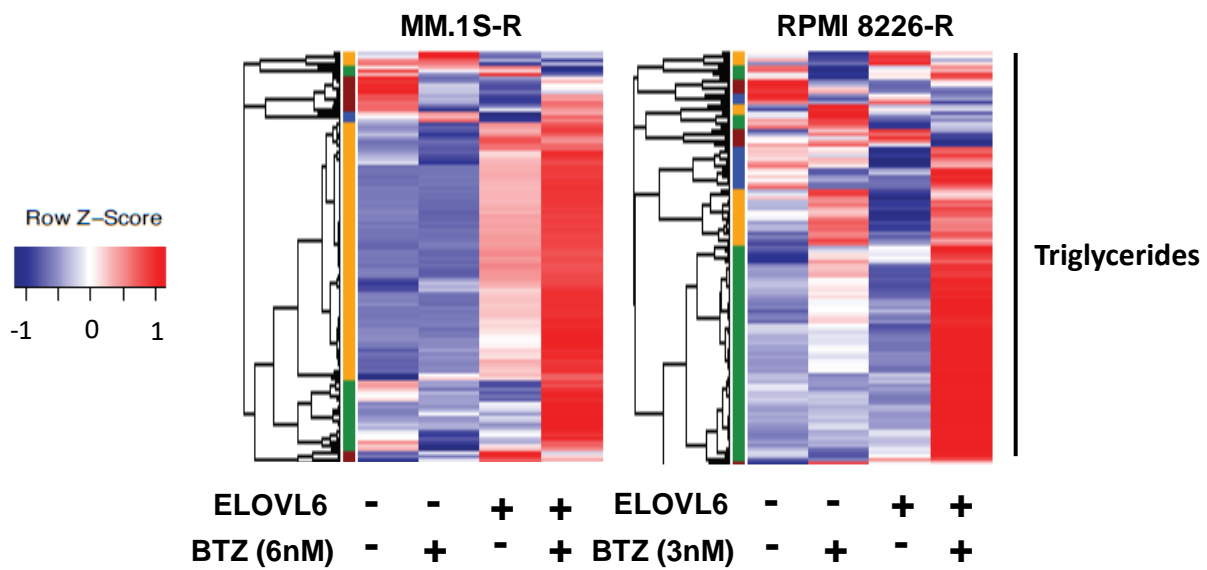
A percent of C12-C16 fatty acyls was calculated for total lipid species that were either upregulated (shown in red in Figure 2G) or downregulated (shown in blue in Figure 2G) in MM.1S and RPMI8226 cells that expressed indicated constructs. Note that a percent of C12-C16 was higher among total lipid species upregulated in ELOVL6-depleted cells and lower among total lipid species downregulated in ELOVL6-depleted cells. The opposite trend is observed for C12-C16 lipids in ELOVL6-overexpressing cells. These data are in agreement with ELOVL6 function in elongation C12-C16 fatty acids.



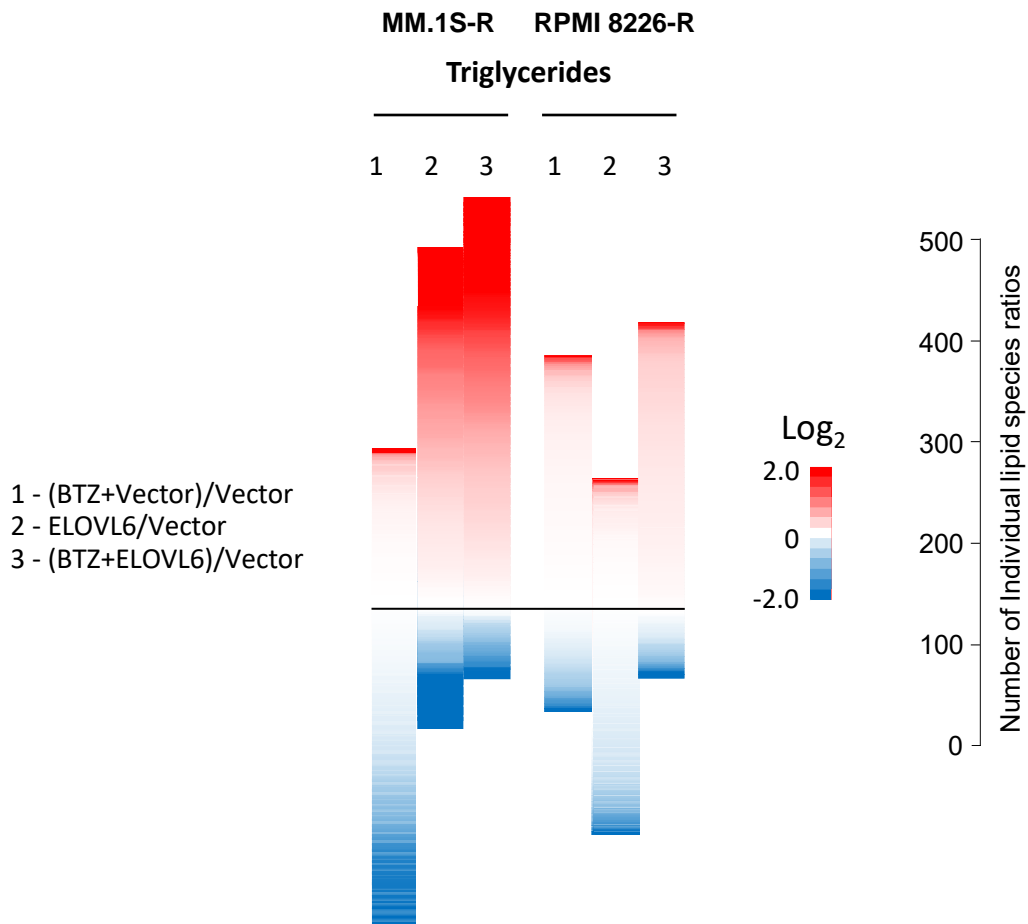
Supplemental Figure 5. Ceramide synthases are induced by BTZ in MM cells

BTZ-resistant MM cells were treated or not with 5nM BTZ and probed in Q-RT-PCR with probes for indicated CERS genes and b-ACTIN. CERS-specific signals were normalized by the corresponding b-ACTIN-specific signals and by their ratio in untreated cells. All data are presented as the mean values of triplicates \pm S.E.M. P-values were determined by Student's t-test. * $p < 0.05$.

A



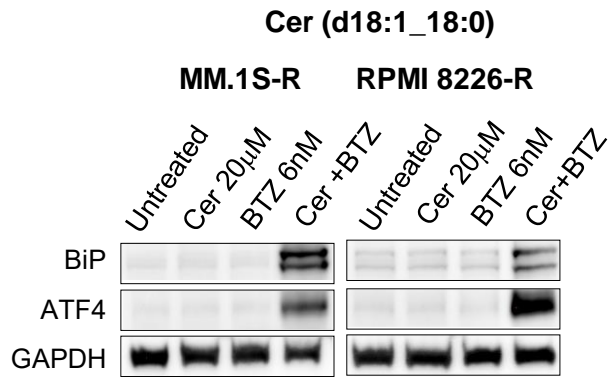
B



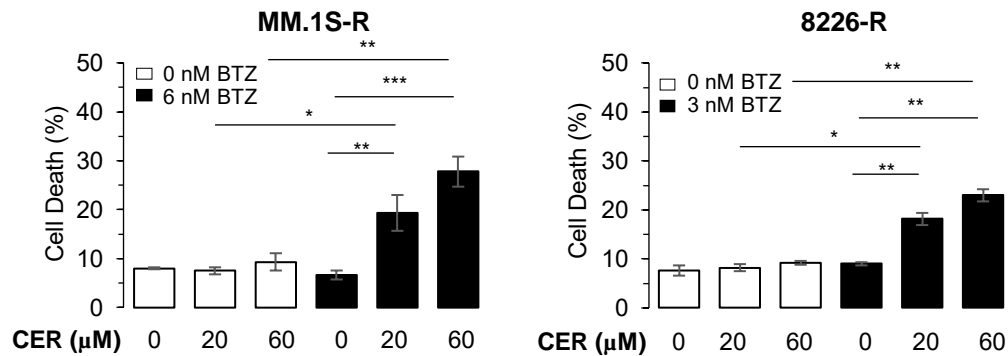
Supplemental Figure 6. ELOVL6 oppositely regulates the majority of triglyceride species in BTZ-resistant cells

A. BTZ-resistant MM cells transduced with empty vector or ELOVL6 were treated or not with the indicated amounts of BTZ for 16hrs followed by lipidomic analysis in independent triplicates. Raw values of each lipid molecule (each row) were transformed as z scores and plotted as a heatmap with red representing the highest value and blue representing the lowest value. **B.** Mean ratios of the levels of individual triglyceride species in designated MM cells were calculated and plotted as heatmaps.

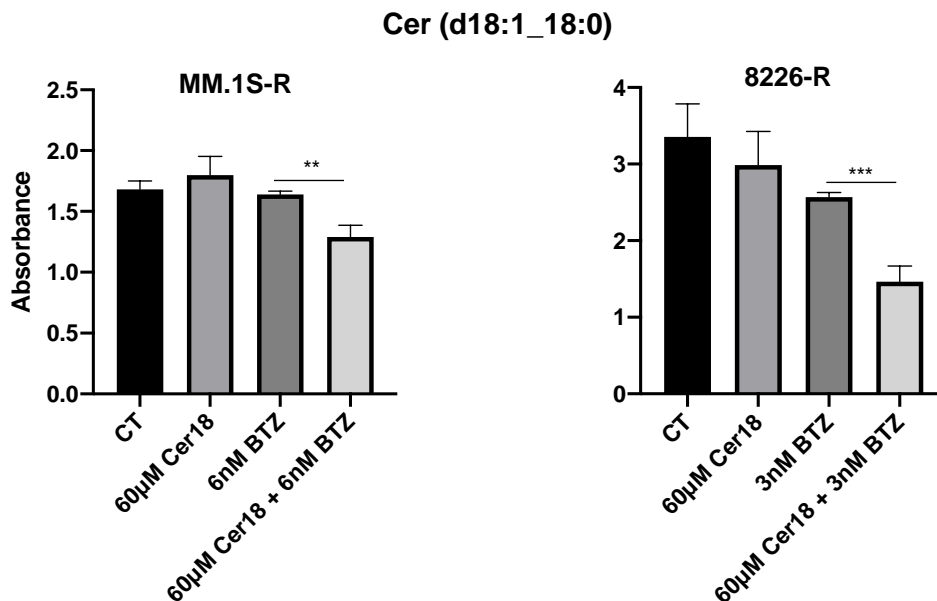
A



B



C



Supplemental Figure 7. Ceramides cooperate with BTZ in inducing ER stress and cell death in BTZ-resistant cells. **A.** BTZ-resistant MM.1S-R and RPMI822-R cells were incubated with d18:1_18:0 ceramide (20 μ M) and/or indicated amounts of BTZ for 16hrs, followed by immunoblotting with indicated antibodies. **B.** BTZ-resistant MM.1S-R and RPMI822-R cells were treated or not with the indicated amounts of d18:1_18:0 ceramide and/or BTZ for 24hrs and probed in trypan blue cell viability assay. **C.** MM.1S-R (left panel) and 8226-R (right panel) were treated with Cer (d18:1_18:0) in the presence or absence of indicated concentrations of BTZ for 24hrs, and cell viability was assessed using the WST-1 cell viability assay.